J. At. Mol. Sci.
doi: 10.4208/jams.012111.012811b

Vol. **2**, No. 2, pp. 99-108
May 2011

Ultrafast photodissociation dynamics of *n*-butyl iodide in the *A*-band

Yu-Zhu Liu, Jin-You Long, Chao-Chao Qin, Ahmed Yousif Ghazal, Yan-Mei Wang, and Bing Zhang*

State Key Laboratory of Magnetic Resonance and Atomic and Molecular Physics, Wuhan Institute of Physics and Mathematics, Chinese Academy of Sciences, Wuhan 430071, China
Graduate School of the Chinese Academy of Sciences, Beijing 100049, China

Received 21 January 2011; Accepted (in revised version) 28 January 2011
Published Online 28 February 2011

Abstract. Ultrafast photodissociation dynamics of *n*-butyl iodide in the *A*-band has been studied by femtosecond time-resolved mass spectroscopy coupled with ion imaging. The time constant of *n*-C_4H_9I in the *A*-band with one photon excitation at ∼267 nm is measured to be ∼(58±6) fs. The ion images of I ($^2P_{3/2}$) and I^* ($^2P_{1/2}$) at ∼267 nm and ∼274 nm are obtained and analyzed to yield corresponding speed and angular distributions. The dependences of dissociation mechanism on excitation wavelength and the size of the alkyl radical are discussed.

PACS: 33.80.Gj, 33.20.-t

Key words: *n*-butyl iodide, ultrafast dynamics, pump-probe, photodissociation, ion imaging

1 Introduction

The photochemistry of alkyl halides in the *A*-band has attracted substantial attention in recent years. One important reason is that it has been realized that halogen atoms and halogen-containing radicals are efficient chemical species for the destruction of stratospheric ozone [1, 2]. Alkyl halides may release halogen atoms or produce halogen-containing radicals following UV absorption. The decay of them in the atmosphere depends largely on their photodissociation rates and product channels in the ultraviolet region. Thus, it is important to determine their photodynamic behavior for assessing their environmental impact. Another reason is that the excited potential energy surfaces (PES) for alkyl halides are known to exhibit multiple surface crossings [3–5]. Together with the spin-orbit interactions, it has made the alkyl halides interesting systems for both theoretical and experimental studies.

*Corresponding author. *Email address:* bzhang@wipm.ac.cn (B. Zhang)

Alkyl iodides are particularly interesting since they offer a unique opportunity to understand the effect of size and structure of the alkyl radicals on the dynamics of dissociation [5]. So far, photodissociation studies in the ultraviolet region have mainly focused on short alkyl iodides [3–12]. As the simplest alkyl iodide, photodissociation of methyl iodide has been the active focus and serves as a paradigm for research into photodissociation processes that occur along a repulsive potential surface of the excited state [6–10]. Other short-chain alkyl iodides such as ethyl iodide (C_2H_5I) [4], *n*-propyl iodide (*n*-C_3H_7I) [11, 12] and *i*-propyl iodide (*i*-C_3H_7I) [11, 12] have also been investigated extensively and intensively in the UV region by ion velocity imaging technique. Compared to short-chain alkyl iodides, *n*-C_4H_9I was less focused as an homologue. Studies on it were rare and only limited to Photofragment Translation Spectroscopy (PTS) [13].

In our previous paper [14], we have reported the effect of branching of α-carbon atom on photodissociation mechanisms of alkyl iodides, which is based on comparison of photodissociation dynamics of *n*-C_4H_9I and *sec*-C_4H_9I at ∼267 nm. As the alkyl group becomes more branched, the mixing of the bending motions about the α-carbon atom with the C–I stretching in the photodissociation of alkyl iodides becomes more significant.

In this paper, we focus on the photodissociation dynamics of *n*-C_4H_9I in the *A*-band in detail, including time constant, the dependences of dissociation mechanism on excitation wavelength and the size of the alkyl radical. With the advent of femtosecond pump-probe technique, the time constant of *n*-C_4H_9I in the *A*-band is measured by time-resolved mass spectroscopy. Using ion imaging technique [15, 16] coupled with resonance enhanced multiphoton ionization (REMPI), the dissociation behavior of *n*-C_4H_9I at ∼267 nm and ∼274 nm is obtained. Each dissociation parameters are compared to get the dependent dissociation mechanism on excitation wavelength. Energy partitioning of *n*-C_4H_9I is compared with small alkyl iodides to get insights into the dependent dissociation mechanism on the size of the alkyl radical.

2 Experimental methods

The experimental setup of the two-dimensional photofragment velocity ion imaging has been described in detail elsewhere [17], which is similar to what Eppink and Parker have reported [15, 16]. Briefly, it consists of a homebuilt time-of-flight mass spectrometer and a two-dimensional position sensitive detector. A molecular beam is produced with a pulsed valve and intersects a linearly polarized tunable ultraviolet laser in the reaction region, which is located in the second stage of the vacuum chamber. The generated ions were extracted and accelerated by the electrostatic immersion lens and projected onto a two-dimensional (2D) detector consisting of two microchannel plates coupled with a P47 phosphor screen and a charge-coupled device camera.

The details of our femtosencond laser system have been described elsewhere [18]. Briefly, the seed beam was generated by a commercial Ti:sapphire oscillator pumped by a CW second harmonic of an Nd:YVO_4 laser, and then amplified by an Nd:YLF pumped regenerative ampli-

fier to generate a 1 kHz pulse train centered at 800 nm of 35 fs pulse width with maximum energy of 1 mJ/pulse. The pump pulse ($\sim$267 nm) was generated in a 0.2 mm thick BBO crystal by sum frequency mixing of the second harmonic and the fundamental. The pump and probe beams were merged by a dichroic mirror and directed into the molecular beam chamber. The time delay between the pump and probe pulses were accurately monitored by a computer-controlled linear translation stage [19].

The UV nanosecond laser was the frequency-doubled output of a dye laser system pumped by the third harmonic of a Nd:YAG (YG981E10, Quantel) and used for both dissociation and state selective ionization of iodine atoms. The atomic fragments were state-selectively detected by a (2+1) REMPI process. The ground state was probed via $7p^4S^0_{3/2} \leftarrow 5p^{5/2}P^0_{3/2}$ transition at 266.49 nm and $6p^2P^0_{3/2} \leftarrow 5p^{5/2}P^0_{3/2}$ transition at 273.78 nm, and the excited state by $np7^0_{3/2} \leftarrow 5p^{5/2}P^0_{1/2}$ transition at 266.62 nm and $9p^4S^0_{3/2} \leftarrow 5p^{5/2}P^0_{3/2}$ transition at 273.54 nm [20].

The liquid sample (*n*-butyl Iodide, 99.9% purity), seeded in helium buffer gas at a background pressure of 2 atm, was expanded through a pulsed valve to generate a pulsed molecular beam. The beam was skimmed and introduced into the ionization chamber where it was intersected perpendicularly by the laser beam.

3 Results and discussion

A femtosecond pump pulse at 267 nm (4.65 eV) is used to excite *n*-butyl Iodide to the *A*-band. Photoexcitation of *n*-butyl Iodide in the *A*-band results in fission of the C–I bond. Two channels of the dissociation are represented by n-$C_4H_9I \rightarrow n$-$C_4H_9 + I/I^*$. Similar as CH_3I [21], a schematic energy diagram with the excited states of n-C_4H_9I discussed above and adiabatic product correlations is shown in Fig. 1. A nuclear wave packet initially prepared in the $^3Q_0$ potential energy curve by a 267 nm femtosecond laser pulse evolves adiabatically on that surface yielding n-$C_4H_9 + I^*(^2P_{1/2})$. A portion of the initial wave packet leaks non-adiabatically to the $^1Q_1$ surface, which correlates with n-C_4H_9+I ($^2P_{3/2}$). Following the real time dynamics of the photodissociation process from reagents to products, time-resolved information of photolysis can be obtained.

Fig. 2 shows the time-resolved total ion signal of the parent ion formed after one-photon excitation of the *A*-band at 267 nm as a function of the pump-probe delay. The decay profiles are fitted with one exponential with time constant of $\sim$(58$\pm$6) fs convoluted with a Gaussian describes the instrument response function. The constant of n-C_4H_9I in the *A*-band is determined to be $\sim$(58$\pm$6) fs.

To gain a further insight into the ultrafast dynamics, photodissociation of n-C_4H_9I is also investigated by ion imaging at $\sim$267 nm and $\sim$274 nm. Fig. 3 shows raw ion images of I and I^* formed upon photolysis of n-C_4H_9I with the laser beam polarized along the vertical direction. The background is removed by subtracting a reference image acquired off molecular beam under the same conditions. As shown in Fig. 4, the speed distributions can be derived by integrating over all angles at each speed by using BASEX technique.

The total released translational energy can be evaluated from the velocity of an individual fragment in the center-of-mass frame. Provided that the velocity of the iodine fragment v is obtained, then the total translational energy E_t is evaluated by

$$E_t = \frac{1}{2}(m_I + m_{C_4H_9})\frac{m_I}{m_{C_4H_9}}v^2, \tag{1}$$

where m_X is the mass of X (X=I, C_4H_9). The available energy for the dissociation process and

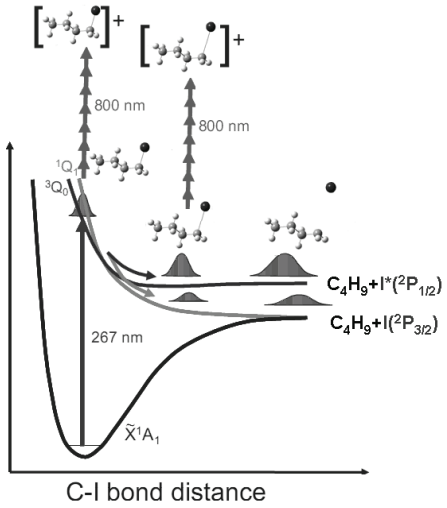

Figure 1: Schematic representation of the relevant potential energy surfaces [21] along the C–I bond representing the *A*-band photodissociation of *n*-C_4H_9I.

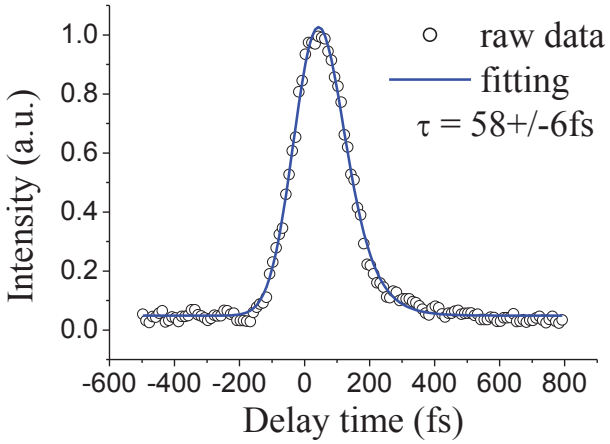

Figure 2: Time-resolved total ion signals of parent ion as a function of delay time between the pump pulse at ~267 nm and the probe pulse at 800 nm. The circles are the experimental results, and solid lines are the fitting results.

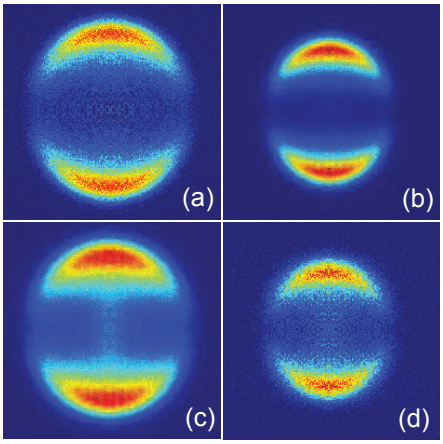

Figure 3: Raw images of (a) I and (b) I^* following the photodissociation of n-C_4H_9I at ~267 nm, (c) I and (d) I^* at ~274 nm.

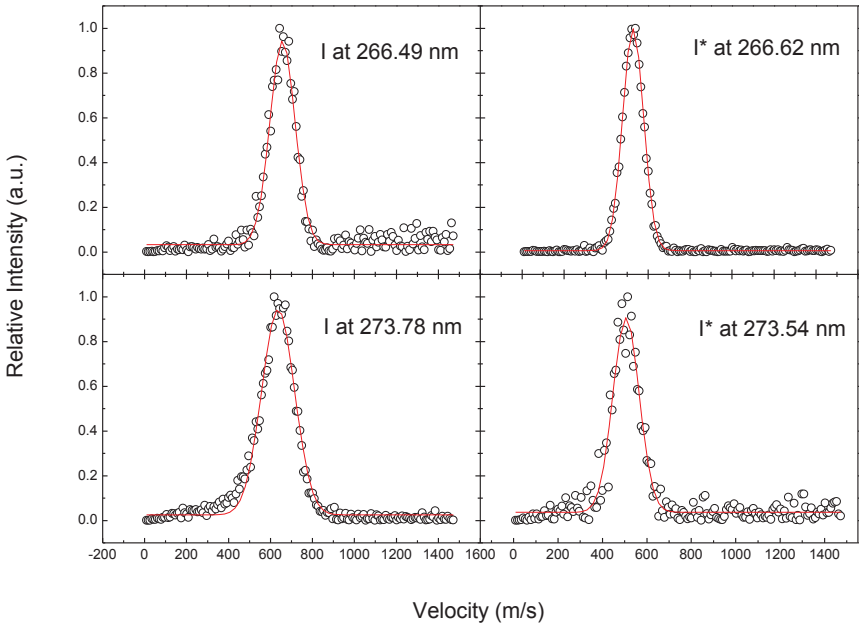

Figure 4: Speed distributions of I and I^* formed upon photolysis of n-C_4H_9I at ~267 nm and ~274 nm. The circles represent the experimental results; the dashed lines show the best-fitting lines.

the internal energy of n-C_4H_9I are calculated by

$$E_{avl} = E_{h\nu} - D_0 + E_{int}^P - E_{el}, \tag{2}$$

where E_{avl} is the available energy, $E_{h\nu}$ is the photon energy, D_0 is the C–I bond dissociation energy evaluated to be 200 kJ· mol^{-1} for n-C_4H_9I [13], E_{el} is the electronic energy level of the

iodine atom, zero for I and 91 kJ·mol^{-1} for I^*, and E_{int}^P is the internal energy of the parent molecule which is considered to be zero under the supersonic molecular beam conditions. The average translational energy $\langle E_t \rangle$ of each component is calculated from the fitting function. The values of $\langle E_t \rangle$ and $\langle E_t \rangle / E_{avl}$ are listed in Table 1.

Table 1: Energy partitioning and velocities of the iodine fragments in the photodissociation of n-C_4H_9I at ∼267 nm and ∼274 nm.

Wavelength (nm)	State	$E_{h\nu}$ (kJ· mol^{-1})	E_{avl} (ms^{-1})	v (kJ·mol^{-1})	$\langle E_T \rangle$ (kJ·mol^{-1})	$\langle E_{int} \rangle$ (kJ·mol^{-1})	$\langle E_t \rangle / E_{avl}$
266.49	I	448.89	248.90	657.09	88.50	160.40	0.356
266.62	I^*	448.68	157.74	528.30	57.21	100.53	0.363
273.78	I	436.94	236.95	636.29	82.99	153.96	0.350
273.54	I^*	437.32	146.38	506.51	52.59	93.79	0.359

The images of I and I^* following the photodissociation of n-C_4H_9I at ∼267 nm and ∼274 nm have shown a simple structure and the corresponding speed distributions can be well fitted by a narrow single-peaked Gaussian curve. Both I and I^* images have much stronger intensities around the poles, suggesting that they should be fragmented mainly as the transition dipole moment is aligned parallel to the C–I bond. The dissociation occurs promptly along the C–I bond after the excitation. The deactivation mechanism of n-C_4H_9I in the A-band is due to prompt dissociation along the C–I stretching via repulsive PES after absorbing one UV photon. The time constant of the A-band of n-C_4H_9I is determined to be ∼(58±6) fs, which reflect prompt dissociation of C–I band in the A-band.

For prompt dissociation, two models have been proposed to represent two limiting cases [6]. One is the rigid model that ignores the flow of energy into the vibrational degrees of freedom of the fragments; the other is the soft radical limit. The fraction of the available energy which has been distributed into the translational energy ($\langle E_t \rangle / E_{avl}$ value) calculated using soft models is 27.9%. As shown in Table 1, the $\langle E_t \rangle / E_{avl}$ values of 35.6% for I and 36.3% for I^* at ∼267 nm, 35.0% for I and 35.9% for I^* at ∼274 nm suggest the soft radical limit of the impulsive model. Consequently, the dissociation dynamics of n-C_4H_9I can be interpreted in terms of the direct dissociation along the C–I stretching and may be expected to result in the high vibrational excitations of n-C_4H_9 fragments.

In Table 1, the internal energy distribution $\langle E_{int} \rangle$ in the n-C_4H_9 radical is more for I^* channel than I channel. It is noteworthy that the translational energy release distributions $\langle E_T \rangle$ corresponding to I and I^* channels extend to substantially lower values as photolysis wavelength increases from ∼267 to ∼274 nm. The dependence of internal energy of n-C_4H_9 fragments on excitation energy can be easily seen from Table 2. As the excitation wavelength increases, the fraction of the available energy distributed into the translational energy decreases. That is to say, more energy is distributed to internal energy of n-C_4H_9 fragments as the excitation energy decreases.

As observed for small alkyl iodides, the fraction of the translational energy release has been measured to be very high, indicating the nonstatistical behavior of dissociation on the

Table 2: The fraction of the available energy which has been distributed into the translational energy ($\langle E_t \rangle / E_{avl}$ value) in the photodissociation of n-C_4H_9I at ~267 nm, ~274 nm and ~277 nm.

Wavelength	$\langle E_t \rangle / E_{avl}$ of I	$\langle E_t \rangle / E_{avl}$ of I^*
~267 nm	35.6%	36.3%
~274 nm	35.0%	35.9%
~277 nm [13]	31.0%	34.3%

repulsive $^3Q_0$ state. However, only about 35% of the available energy is released in translation at the two wavelengths studied in the photolysis of n-C_4H_9I. For comparison, the fraction of the translational energy release of alkyl iodides (including CH_3I [6], C_2H_5I [4], n-C_3H_7I [12] and n-C_4H_9I) in the photolysis of ~267 nm is shown in Fig. 5. It suggests that the long alkyl structure produces a quite inefficient energy disposal to the translational motion of photofragments. The trend toward increased internal excitation with the size of the alkyl radical is indicative of the structure dependence on the dynamics of molecular processes.

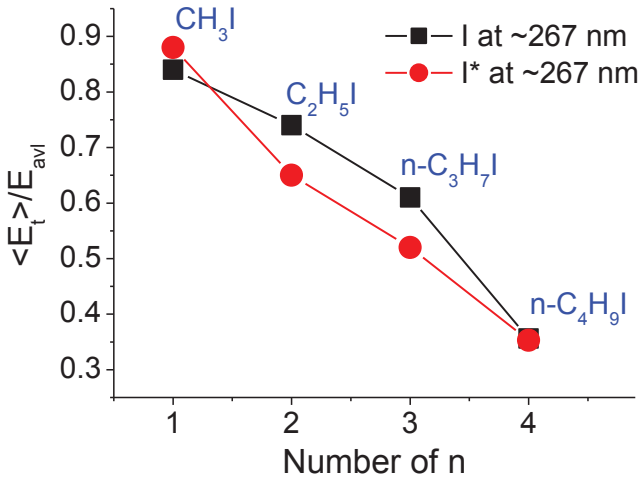

Figure 5: The fraction of the translational energy release of alkyl iodides (n-$C_nH_{2n+1}I$) in the photolysis of ~267 nm.

Angular distributions of the fragments $I(\theta)$ can be extracted by integrating the reconstructed three-dimensional spatial distribution over a proper range of speed at each angle. It can be characterized by anisotropy parameter β as expressed by

$$I(\theta) = (4\pi)^{-1}\left(1+\beta P_2(\cos\theta)\right), \tag{3}$$

where $P_2(\cos\theta)$ is the second-order Legendre polynomial, θ is the angle between the laser polarization direction and the recoil velocity of fragments, and β is constrained between 2 (parallel transition) and -1 (perpendicular transition). In this manner, the value of anisotropy

parameter β for I and I^* channels are obtained ($\beta(I)=1.42\pm0.05$, $\beta(I^*)=1.91\pm0.05$ at $\sim$267 nm and $\beta(I)=1.48\pm0.1$, $\beta(I^*)=1.24\pm0.1$ at $\sim$274 nm).

It is interesting to note that the value of $\beta(I^*)$ are substantially less anisotropic than that of $\beta(I)$ at $\sim$274 nm photolysis. Polar plots of angular distributions of (a) I and (b) I^* fragments from n-C_4H_9I at $\sim$274 nm are shown in Fig. 6. Generally, for small alkyl iodides such as CH_3I [3], C_2H_5I [4], and n-C_3H_7I [12], the values of $\beta(I^*)$ are bigger than that of $\beta(I)$ at the same wavelength. However, as the alkyl radical becomes heavier, for example, n-$C_5H_{11}I$ [22], and c-$C_6H_{11}I$ [23], the value of β shows the characteristic of $\beta(I)$ bigger than $\beta(I^*)$. This difference indicates that the value of β for I^* at the corresponding excitation wavelength is less than that for I as the alkyl radical becomes heavier [13].

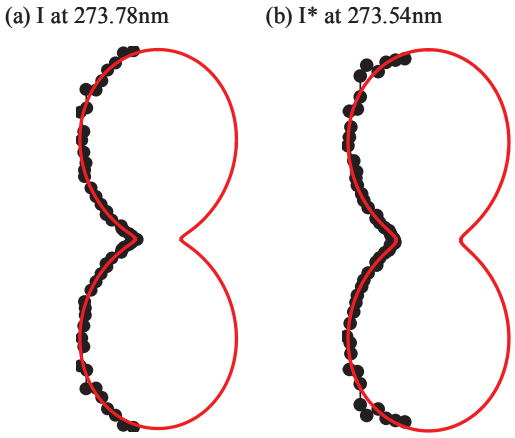

Figure 6: Polar plots of angular distributions of (a) I and (b) I^* fragments from n-C_4H_9I at $\sim$274 nm. The linear polarizations of the pump and probe lasers are aligned vertical in the plane of the figure. The dots are the experimental results, and red lines are the corresponding fits using Eq. (3). The fitting results are (a) $\beta(I)=1.48\pm0.1$, (b) $\beta(I^*)=1.24\pm0.1$.

As to n-C_4H_9I itself, $\beta(I)$ decreases while $\beta(I^*)$ increases as the wavelength increases, as shown in Table 3. The dependence of β on wavelength can be explained in terms of the contribution ratios of the parallel and the perpendicular transition to the product. Three states $^3Q_0$, $^3Q_1$, and $^1Q_1$ in Mulliken's notation [24] are considered in the photolysis of alkyl iodides. The $^3Q_0$ state correlates with the I^* product and the dipole moment is aligned parallel to the C–I bond, while the $^3Q_1$, and $^1Q_1$ states lead to the I formation through perpendicular transition.

Here, we take I^* channel as an example for discussion. Due to curve crossing between the $^1Q_1$ and $^3Q_0$ states, the A-band excitation leads to I^* product via two channels: (1) excited directly to the $^3Q_0$ state and dissociate (parallel transition); (2) excited to the $^1Q_1$ state, partially coupled to the $^3Q_0$ state and dissociate (perpendicular transition). The contribution ratios of the parallel ($x_{//}$) and perpendicular transitions ($x_{\perp}$) can be obtained from β value for each photolysis channel [3], which is also shown in Table 3. It is clearly seen that the

Table 3: Anisotropy parameter β for I and I^* channels and the contribution ratios of the parallel ($R_{//}$) and perpendicular transitions ($R_\perp$) of each channel in the photodissociation of n-C_4H_9I in the A-band.

Wavelength	$\beta(I)$	Contribution	$\beta(^*)$	Contribution
~267 nm	1.42±0.05	$x_{//}$=0.81 $x_\perp$=0.19	1.91±0.05	$x_{//}$=0.97 $x_\perp$=0.03
~274 nm	1.48±0.1	$x_{//}$=0.83 $x_\perp$=0.17	1.24±0.1	$x_{//}$=0.75 $x_\perp$=0.25
~277 nm [13]	1.60±0.1	$x_{//}$=0.87 $x_\perp$=0.13	0.90±0.1	$x_{//}$=0.63 $x_\perp$=0.37

contribution ratio of the perpendicular transition ($x_\perp$) for I^* channel increases as the excitation wavelength. Therefore, the increasing of $\beta(I^*)$ is ascribed to the increasing of curve crossing between the $^1Q_1$ and $^3Q_0$ states as the excitation wavelength. The mechanism of the decreasing of $\beta(I)$ is the similar, which is due to the increasing of curve crossing between the $^3Q_0$ and $^1Q_1$ states as the excitation wavelength. It can be concluded that the non-adiabatic coupling increases between electronic states as the excitation wavelength.

4 Conclusions

Ultrafast photodissociation dynamics of n-butyl iodide in the A-band has been studied by femtosecond time-resolved mass spectroscopy coupled with ion imaging. The time constant of n-C_4H_9I in the A-band with one photon excitation at ~267 nm is measured to be ~(58±6) fs. The ion images of I ($^2P_{3/2}$) and I^* ($^2P_{1/2}$) at ~267 nm and ~274 nm are obtained and analyzed. The photodissociation processes occur along the C–I stretching via repulsive potential surface after absorbing one UV photon. More energy is distributed to internal energy of n-C_4H_9 fragments as the excitation energy decreases. At the same time, the fraction of available energy distributed to internal energy increases as the size of the alkyl radical increase. It is indicative of the structure dependence on the dynamics of molecular processes. In addition, the non-adiabatic coupling increases between electronic states as the excitation wavelength.

Acknowledgments. The project was supported by the National Natural Science Foundation of China under Grant No. 20973194 and Innovation Foundation of Chinese Academy of Sciences under Grant No. KJCX1-YW-N30.

References

[1] S. C. Wofsy, M. B. McEloroy, and Y. L. Yung, Geophys. Res. Lett. 2 (1975) 215.
[2] Y. L. Yung, J. P. Pinto, R. J. Watson, and S. P. Sander, J. Atmos. Sci. 37 (1980) 339.
[3] A. Eppink and D. H. Parker, J. Chem. Phys. 109 (1998) 4758.
[4] Y. Tang, W. B. Lee, Z. Hu, B. Zhang, and K. C. Lin, J. Chem. Phys. 126 (2007) 064302.
[5] S. Uma and P. K. Das, J. Chem. Phys. 104 (1996) 4470.
[6] S. J. Riley and K. R. Wilson, Faraday Discuss. Chem. Soc. 53 (1972) 132.

[7] H. Guo and G. C. Schatz, J. Chem. Phys. 93 (1990) 393.
[8] Y. J. Jung, Y. S. Kim, W. K. Kang, and K. H. Jung, J. Chem. Phys. 107 (1997) 7187.
[9] A. V. Baklanov, M. Aldener, B. Lindgren, and U. Sassenberg, Chem. Phys. Lett. 325 (2000) 399.
[10] A. Eppink and D. H. Parker, J. Chem. Phys. 110 (1999) 832.
[11] H. Y. Fan and S. T. Pratt, J. Chem. Phys. 123 (2005) 204301.
[12] F. Zhang, Z. Z. Cao, X. Qin, *et al.*, Acta Phys. -Chim. Sin. 24 (2008) 1335 (in Chinese).
[13] W. K. Kang, K. W. Jung, and K. H. Jung. J. Phys. Chem. 98 (1994) 1525.
[14] Y. Liu, Q. Zhang, Y. Zhang, *et al.*, ChemPhysChem. 10 (2009) 830.
[15] A. Eppink and D. H. Parker, Rev. Sci. Instrum. 68 (1997) 3477.
[16] D. H. Parker and A. Eppink. J. Chem. Phys. 107 (1997) 2357.
[17] Y. Tang, L. Ji, B. F. Tang, *et al.*, Acta Phys. -Chim. Sin. 20 (2004) 344 (in Chinese).
[18] Z. Wei, F. Zhang, Y. Wang, and B. Zhang, Chinese J. Chem. Phys. 20 (2007) 419.
[19] Y. Liu, B. Tang, H. Shen, *et al.*, Opt. Express 18 (2010) 5791.
[20] R. J. Donovan, R. V. Flood, K. P. Lawley, *et al.*, Chem. Phys. 164 (1992) 439.
[21] J. Durá, R. de Nalda, G. A. Amaral, and L. Bañares, J. Chem. Phys. 131 (2009) 134311.
[22] Y. Zhang, J. Wang, Q. S. Zheng, *et al.*, Acta Phys. -Chim. Sin. 25 (2009) 661 (in Chinese).
[23] R. Zhang, A. Y. Ghazal, Y. Liu, *et al.*, Opt. Commun. 282 (2009) 2169.
[24] R. S. Mulliken, J. Chem. Phys. 8 (1940) 382.